Journal of Organometallic Chemistry 694 (2009) 2757–2769

Contents lists available at ScienceDirect

Journal of Organometallic Chemistry

journal homepage: www.elsevier.com/locate/jorganchem

Synthesis and characterization of cyclometalated iridium(III) complexes containing pyrimidine-based ligands

Cing-Fong Lin [a], Wei-Sheng Huang [b], Hsien-Hsin Chou [b], Jiann T. Lin [a,b,*]

[a] Department of Chemistry, National Central University, Chungli 320, Taiwan
[b] Institute of Chemistry, Academia Sinica, Taipei 11529, Taiwan

ARTICLE INFO

Article history:
Received 10 February 2009
Received in revised form 1 April 2009
Accepted 2 April 2009
Available online 19 April 2009

Keywords:
Iridium(III) complexes
Phosphorescence
Pyrimidine
Light-emitting diodes

ABSTRACT

New pyrimidine derivatives (**pyr**) have been synthesized using palladium-catalyzed Suzuki coupling reaction. These compounds can undergo cyclometalation with iridium trichloride to form bis-cyclometalated iridium complexes, (**pyr**)$_2$Ir(acac) (acac = acetylacetonate; **pyr** = cyclometalated **pyr**). The substituents at the both cyclometalated phenyl ring and pyrimidine ring were found to affect both electrochemical and photophysical properties of the complexes. Computation results on these complexes are consistent with the electrochemical and photophysical data. The complexes are green-emitting with good solution quantum yields at ~0.30. Light-emitting devices using these complexes as dopants were fabricated, and the device performance at 100 mA/cm^2 are moderate: **9** (17 481 cd/m^2, 4.8%, 18 cd/A, 5.1 lm/W); **10** (18 704 cd/m^2, 4.9%, 18.9 cd/A, 4.7 lm/W); **13** (20 942 cd/m^2, 5.4%, 21.0 cd/A, 6.1 lm/W).

1. Introduction

Transition-metal-based phosphorescent complexes have received considerable attention in recent years because of their potential application in organic light-emitting diode (OLED) [1]. Strong spin–orbital coupling induced by the heavier metal ion results in mixing of the singlet and triplet excited states and leads to high phosphorescence efficiency due to removal of the spin-forbidden constraint of the radiative relaxation of triplet state [2]. Among phosphorescent metal complexes, iridium(III) complexes appear to be the most intensively explored owing to their easy syntheses and excellent color tunability [3]. A large number of iridium complexes reported in literature contained two cyclometalated ligands, such as 2-phenylpyridine [4], quinozaline [5], phenyltriazole [6] and 2-phenylbenzoimidazole [7], together with an auxiliary ligand such as acetylacetonate (acac) or picolinate (pic). High performance phosphorescent OLEDs were achieved using these phosphorescent dyes as dopants in a small molecule [5–8] or polymer host [9].

We have been interested in the development of new phosphorescent metal complexes for applications in OLEDs. Series of complexes with cyclometalated benzimidazole-based [7a,10] and lepidine-based [11] ligands were successfully synthesized and OLEDs using these complexes were also demonstrated. In this report, we extended our research to cyclometalated pyrimidine-based ligands. Pyrimidine, an important motif in natural products [12], has also been used in materials such as liquid crystals [13] and OLEDs [14]. Pyrimidine is expected to be more electron-deficient than its pyridine congener which has been used to construct electron-transporting materials [15]. Cyclometalation with pyrimidine-containing ligands may possibly afford complexes which are color tunable and capable of electron transporting. In this article, we systematically designed and synthesized a series of new pyrimidine-based iridium complexes which have cyclometalated electron-donating (4-*tert*-butyl, 4-methoxy, 2-thiophenyl) or electron-withdrawing (4-trifluormethyl, 4-fluoro, 3-trifluoromethyl) aromatic rings at positions 2 and/or 5 of the pyrimidine moiety. To our knowledge, there were only two reports on pyrimidine-based iridium complex with cyclometalated aromatic ring residing at position 4 of the pyrimidine moiety [16]. The electrochemical, photophysical and electrophosphorescent properties of these iridium complexes will be discussed.

2. Results and discussion

2.1. Synthesis of the materials

The synthetic routes and chemical structures of the pyrimidine derivatives are shown in Scheme 1 and Chart 1 respectively. The starting material, 5-bromo-2-iodopyrimidine, was synthesized by following the literature procedures [17]. The preparation of pyrimidine ligands (abbreviated as **pyr**) involved a two-step synthesis from 5-bromo-2-iodopyrimidine: (1) carbon–carbon bond formation via palladium-catalyzed Suzuki cross-coupling with the corresponding arylboronic acid at the iodo-substituted carbon; (2) a

* Corresponding author. Address: Department of Chemistry, National Central University, Chungli 320, Taiwan. Tel.: +886 2 27898522; fax: +886 2 27831237.
E-mail address: jtlin@chem.sinica.edu.tw (J.T. Lin).

0022-328X/$ - see front matter © 2009 Elsevier B.V. All rights reserved.
doi:10.1016/j.jorganchem.2009.04.011

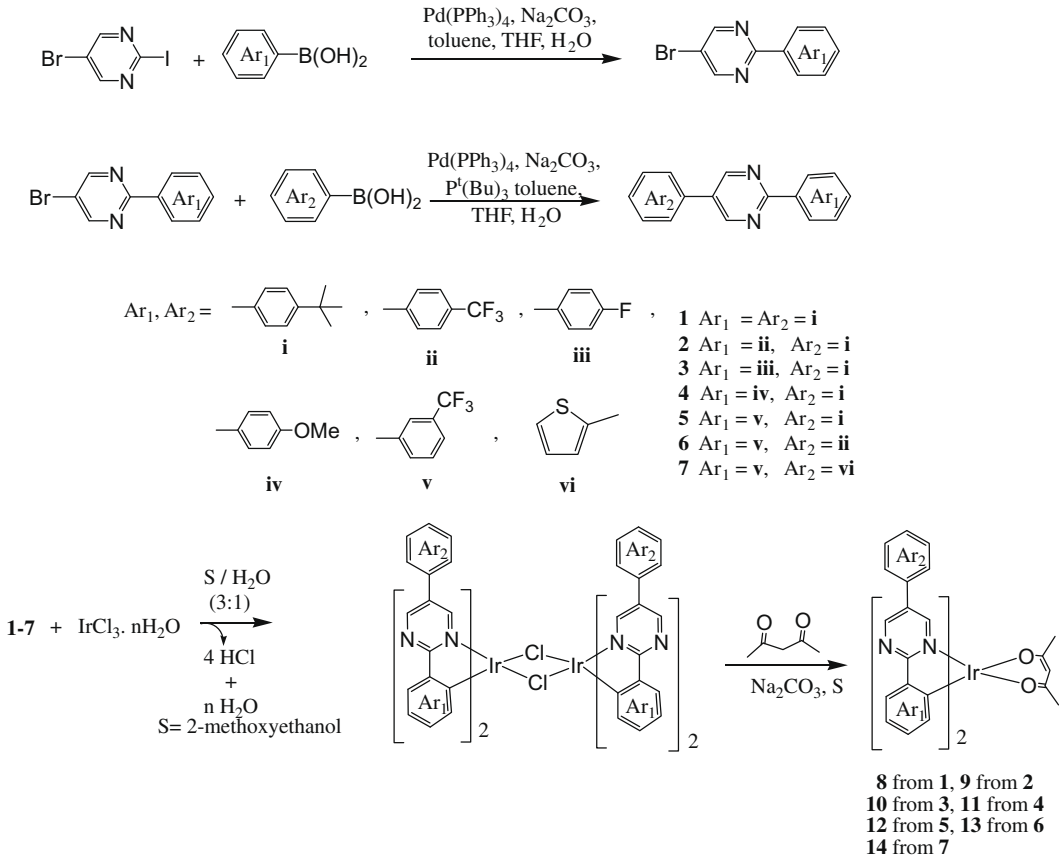

Scheme 1. Synthetic of the pyrimidine ligands and their iridium complexes.

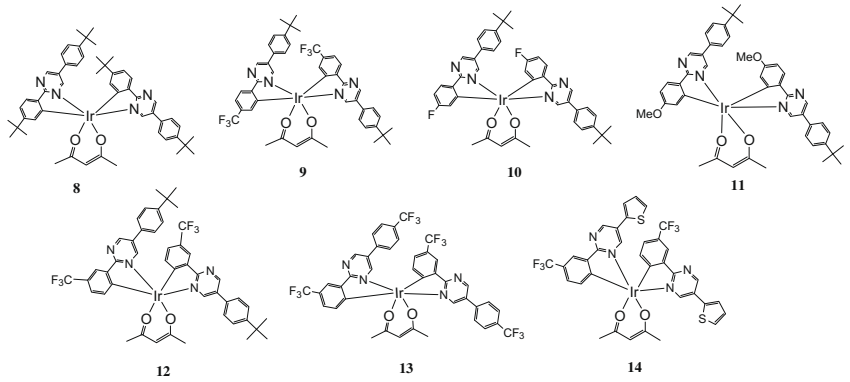

Chart 1. Molecular structures of compound **8–14**.

second Suzuki coupling with another arylboronic acid at the bromo-substituted carbon. A bulky phosphine, P^tBu_3, was adding as the cocatalyst [14a]. The preparation of cyclometalated iridium complexes, (**pyr**)$_2$Ir(acac) (**pyr** is the cyclometalated ligand), involved a two-step synthesis: (1) $IrCl_3 \cdot nH_2O$ reacted with **pyr** to form a chloro-bridged dimmer; (2) the dimer was then treated with 2,4-pentanedione in the presence of base to form (**pyr**)$_2$Ir(acac).

2.2. Electrochemical properties

The electrochemical properties of (**pyr**)$_2$Ir(acac) were studied using cyclic voltammetry (CV), and the electrochemical data are summarized in Table 1. The cyclic voltammograms of the complexes are shown in Fig. 1. The energies of the highest occupied molecular orbitals (HOMOs) in (**pyr**)$_2$Ir(acac) were calculated relative to ferrocene (Fc) which has a value of −4.8 eV with respect to the vacuum level [18]. The HOMO energies in combination with the optical bandgaps derived from the absorption band edges were used to calculate the energies of the lowest unoccupied molecular orbitals (LUMOs) of the iridium complexes. Both HOMO and LUMO energies are collected in Table 1.

No chemically reversible reduction waves were detected for (**pyr**)$_2$Ir(acac). In comparison, a quasi-reversible one-electron oxidation wave ranging from 772 to 1424 mV (versus Ag/$AgNO_3$) was observed in each complex. This is attributed to the oxidation of the iridium(III) based on previous electrochemical studies and theoretical calculations [6,19]. These values appear to be high compared to those of (ppy)$_2$Ir(acac) (ppy = 2-phenylpyridine) [20],

Table 1
Photophysical and electrochemical data for (**pyr**)$_2$Ir(acac) and **pyr**.

Compounds	λ_{abs} (log ε)[a] (nm)	λ_{em}[b] (nm)	Φ_p[c]	τ[d] (μs)	τ_r,[e] μs	E_{ox}[f] (mV)	HOMO[g] (eV)	LUMO[h] (eV)	E_g[i] (eV)
1	296 (4.9)								
2	292 (4.9)								
3	290 (4.96)								
4	306 (4.97)								
5	291 (4.92)								
6	282 (4.94)								
7	313 (4.97)								
8	277 (4.93), 307 (4.5), 380 (4.0), 438 (3.8)	544	0.28	1.16	4.13	772 (110)	−5.28	3.0	2.28
9	304 (4.92), 380 (4.3), 435 (4.0), 472 (3.5)	542	0.29	2.39	8.24	1047 (110)	−5.55	3.29	2.27
10	306 (4.91), 367 (4.2), 418 (4.0)	522	0.34	2.15	6.32	994 (100)	−5.50	3.10	2.40
11	275 (5.07), 318 (4.90), 376 (4.2), 430 (3.1)	532	0.32	2.26	7.06	855 (120)	−5.35	2.92	2.41
12	275 (5.07), 301 (4.91), 375 (4.0), 425 (3.8)	526	0.27	1.49	5.52	1360 (110)	−5.86	3.26	2.33
13	277 (5.05), 378 (4.4), 425 (4.0), 462 (3.8)	531	0.32	1.30	4.06	1422 (100)	−5.92	3.32	2.33
14	327 (4.8), 385 (4.07), 446 (3.5)	558	0.052	4.18	80.4	1387 (110)	−5.88	3.37	2.25

[a] Measured in CH_2Cl_2 10^{-5} M at 298 K. ε is the absorption coefficient.
[b] Recorded in toluene solutions at 298 K. Excitation wavelength was 400 nm for all iridium compounds.
[c] Quantum yield was measured with respect to coumarin (Φ_{em} = 0.63 in acetonitrile).
[d] Measured at 298 K. Excitation wavelength was 350 nm.
[e] $\tau_r = \tau/\Phi_p$.
[f] Oxidation potentials reported are referenced to $Ag/AgNO_3$. The values in parenthesis are the difference between the cathodic and anodic peaks. Conditions of cyclic voltammetric measurements: platinum working electrode; $Ag/AgNO_3$ reference electrode. Scan rate: 100 mV/s. Electrolyte: tetrabutylammonium hexafluorophosphate.
[g] HOMO levels calculated from CV potentials using ferrocene as a standard [HOMO = − 4.8 + ($E_{Fc} - E_{ox}$)].
[h] LUMO levels derived via equation E_g = LUMO − HOMO.
[i] E_g: bandgap. E_g was obtained from the absorption spectra.

$(ppy)_3Ir$ [21,22] and analogues, and $(ppy)_2Ir(L)^+$ (L = 2,2′-bipyridine) and analogues [23] as well. The highest occupied molecular orbital (HOMO) of $(ppy)_2Ir(acac)$ was demonstrated to consist principally of a mixture of the 5d orbital of Ir and the phenyl-π orbital of ppy [24]. Accordingly, variation of the substituents at the cyclometalated phenyl ring will affect the oxidation potential of the iridium ion in the congeners of $(ppy)_2Ir(acac)$ [20]. The HOMO of (**pyr**)$_2$Ir(acac) also consists mainly of the 5d of Ir and the cyclometalated phenyl-π orbital based on the computation results (vide infra). Therefore, the oxidation potential of Ir(III) in (**pyr**)$_2$Ir(acac) is expected to have a similar trend with that of $(ppy)_2Ir(acac)$. Complexes **12** and **9** have an electron-withdrawing CF_3 unit at positions 4 and 3 (Fig. 2) of the cyclometalated phenyl ring, respectively. However, the former has a higher oxidation potential (1360 versus 1047 mV). This may be rationalized by the larger Hammett parameter σ of CF_3 unit in **12**, which is at the *para* position of the Ir atom [25] and more effectively depletes the electron density of the Ir atom. Complexes **8–11**, having a different substituent at position 3 (Fig. 2) of the cyclometalated phenyl ring, have the oxidation potentials in the order of **8** (772 mV) < **11** (855 mV) < **10** (994 mV) < **9** (1047 mV). This is consistent with the order of Hammett parameter σ_{meta} [25], CMe_3 (−0.09) < OMe (0.10) < F (0.34) < CF_3 (0.46). The substituent at position 4 (*meta* to the ligated nitrogen atom) of the pyrimidine ring in **pyr** also affects the oxidation potential of the iridium ion, though to a lesser extent. For complexes **12–14** which have a different substituent at position 4 of the pyrimidine ring, the oxidation potentials increase in the order of **12** (1360 mV) < **14** (1387 mV) < **13** (1422 mV). This is consistent with the order of Hammett parameter for the *meta*-substituent. Possibly more electron-deficient nitrogen atom lowers the energy level of the metal because of stronger metal-to-ligand charge-transfer.

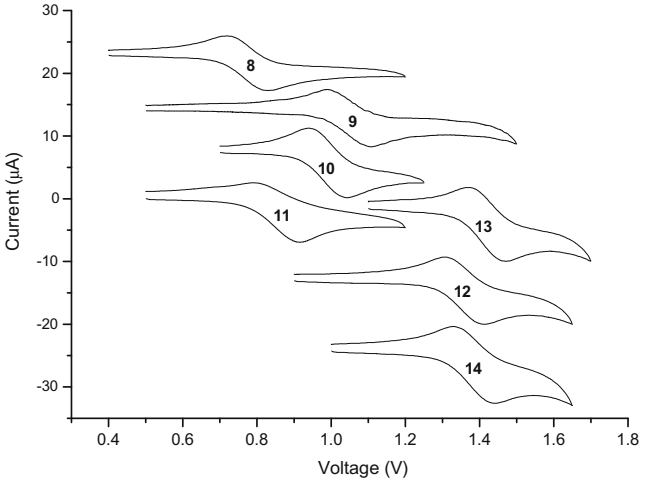

Fig. 1. Cyclic voltammograms of **8–14**, measured in CH_2Cl_2.

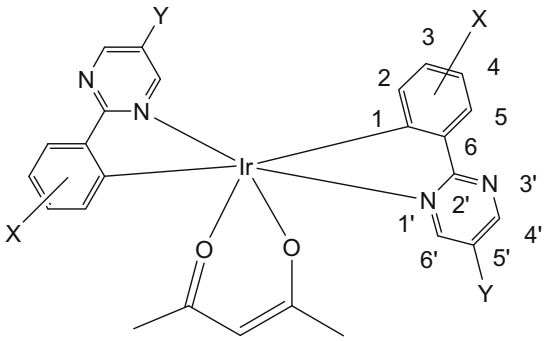

Fig. 2. The structure of (**pyr**)$_2$Ir(acac) with labeling at the cyclometalated phenyl ring.

2.3. Photophysical properties

The photophysical data of **pyr** and (**pyr**)$_2$Ir(acac) are collected in Table 1. Absorption spectra for selected free ligands and (**pyr**)$_2$Ir(acac) complexes are shown in Fig. 3. The strong absorption bands of the **pyr** ligands observed at about 250–350 nm with high extinction coefficients (ε > 80 000 M^{-1} cm^{-1}) are mainly due to π–π* transitions. Ligands with electron-donating substituents such as OMe (**4**) and thiophene ring (**7**) have a longer absorption wavelength than others, possibly there exists weak charge-transfer

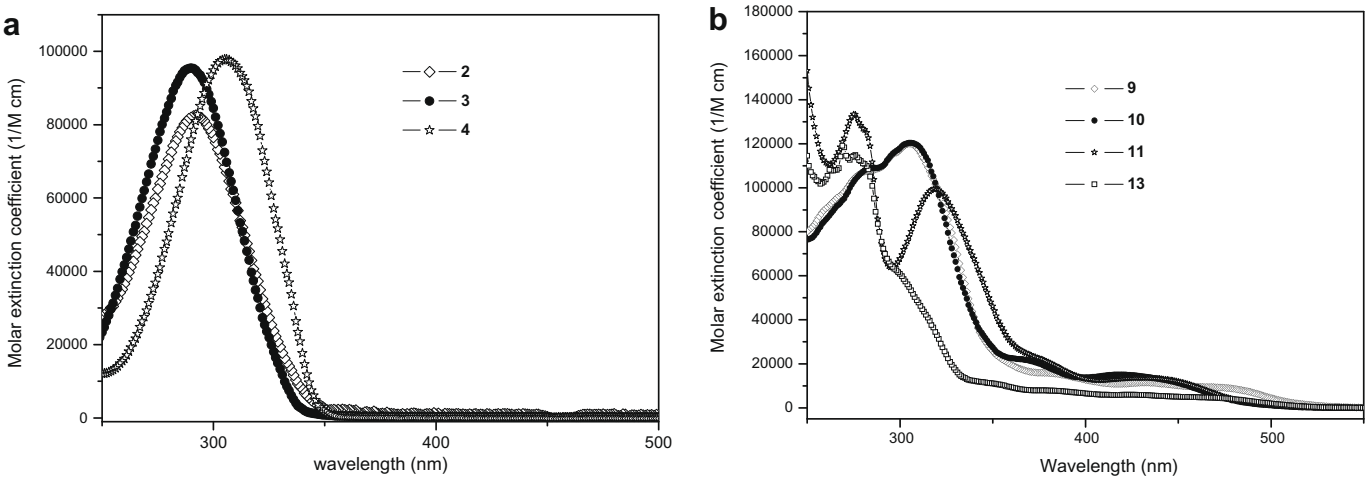

Fig. 3. Absorption spectra of compounds in CH_2Cl_2 (a) **pyr** ligands and (b) (**pyr**)$_2$Ir(acac).

from these electron donors to the electron-deficient acceptor, pyrimidine. Ligand (**6**) with two electron-withdrawing substituents, CF_3, appears to have the shortest absorption wavelength. The strong absorption bands of complexes (**pyr**)$_2$Ir(acac) at about 250–380 nm with high extinction coefficients are assigned to the π–π^* transitions of the **pyr** ligands by comparison with the absorption spectra of the corresponding **pyr** ligands. The absorption bands at 380–520 nm can be assigned to the spin-allowed metal-to-ligand charge-transfer (^{1}MLCT) and the spin-forbidden ^{3}MLCT bands. As aforementioned, the substituent affects the HOMO energy level in the complexes. The LUMO energy level, being delocalized over the whole ligand π orbitals (vide infra), is also affected by the substituent. Therefore, it is less easy to rationalize the trend of ^{1}MLCT and ^{3}MLCT energies.

The **pyr** ligands emit in the violet-blue region. In contrast, the emission wavelengths of (**pyr**)$_2$Ir(acac) fall in the range of λ_{em} = 522–558 nm, which vary with the structures of the cyclometalated ligands. All phosphorescence spectra of (**pyr**)$_2$Ir(acac) are shown in Fig. 4. The prominent vibronic feature of the emission spectra indicates that there is significant mixing of the ^{3}MLCT and $^3\pi\pi^*$ transitions. It was reported that an inductive-only electron-withdrawing CF_3 group at positions 4 and 2 of the cyclometalated phenyl ring (Fig. 2) will lead to electron deficiency of position 1 and result in hypsochromic shift of the emission [26]. Such an outcome was attributed to the lowering of the σ-donation from the cyclometalated ligand, i.e., lowering of the HOMO level. Conversely, CF_3 group at positions 3 and 5 of the cyclometalated phenyl ring will render position 1 of the aromatic ring less electron deficient. We observed similar phenomena: λ_{em} **(12)** < λ_{em} **(9)** It was also reported that fluorine atom behaved differently from CF_3 group because of its mesomeric and inductive nature [26]. Indeed, the complex **10** was found to have a shorter emission wavelength than not only **9**, but also **8** which has an inductive-only electron-donating *tert*-butyl group in position 3. It is believed that the shorter emission wavelength of **11** (λ_{em} = 532 nm) than **8** (λ_{em} = 544 nm) is due to the mesomeric and inductive nature of the OMe group [25]. These results are also supported by the molecular orbital calculations (vide infra). Complexes **12**–**14** have the same cyclometalated phenyl ring but different substituents at position 5 of the pyrimidine. The order of λ_{em} values, **12** < **13** < **14**, implies that the LUMO level also plays an important role in color tuning. Though the substituent at position 5' of pyrimidine can only have inductive effect on the ligated nitrogen (vide supra) of pyrimidine, it is believed that the thiophene ring is beneficial to lowering the energy of the π^* orbital of **pyr** ligand via delocalization.

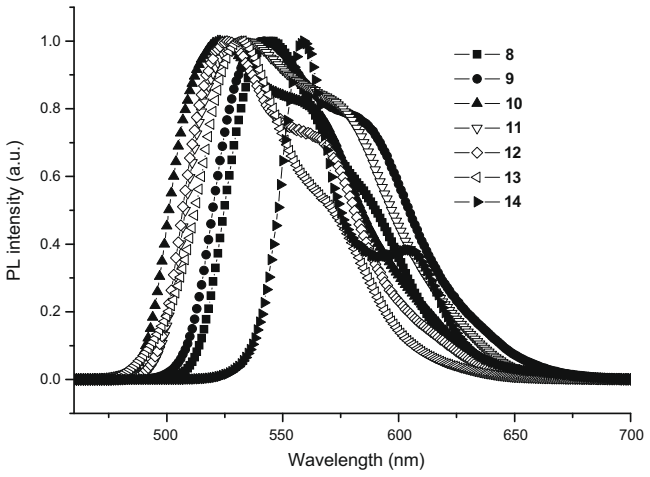

Fig. 4. Phosphorescence spectra of all complexes in toluene at 298 K.

Except for **14** (Φ_p = 0.052), most of (**pyr**)$_2$Ir(acac) exhibit good solution phosphorescence quantum yields (Φ_p = 0.28–0.34) at room temperature under air free condition, indicating that there exists strong spin–orbit coupling. The relatively low quantum yield of **14** is supported by the significantly larger non-radiative decay rate constant than the radiative constant (22 versus $1.2 \times 10^4\ s^{-1}$). The observed phosphorescence lifetimes of ca. 1.16–4.18 μs in degassed toluene for all complexes were used to deduce the radiative lifetimes of 4.14–80.4 μs via the equation $\tau_r = \tau/\Phi_{em}$. The complexes should be appropriate for phosphorescent OLEDs because of their short excited state lifetimes and high phosphorescence quantum yields.

2.4. MO calculation

Molecular orbital calculations using Q-Chem (see Experimental section) [27] on selected complexes were carried out to gain more insight into the photophysical properties of the complexes. The features of the three highest occupied (HOMO, HOMO − 1, and HOMO − 2) and the three lowest unoccupied (LUMO, LUMO + 1, and LUMO + 2) frontier orbitals mainly involved in the transition are depicted in Fig. 5, and the description and energy gaps of each transition are listed in Table 2. The electron densities of the HOMO and HOMO − 1 are located mainly on the metal, acetylacetonate and the cyclometalated phenyl ring, whereas the LUMO and

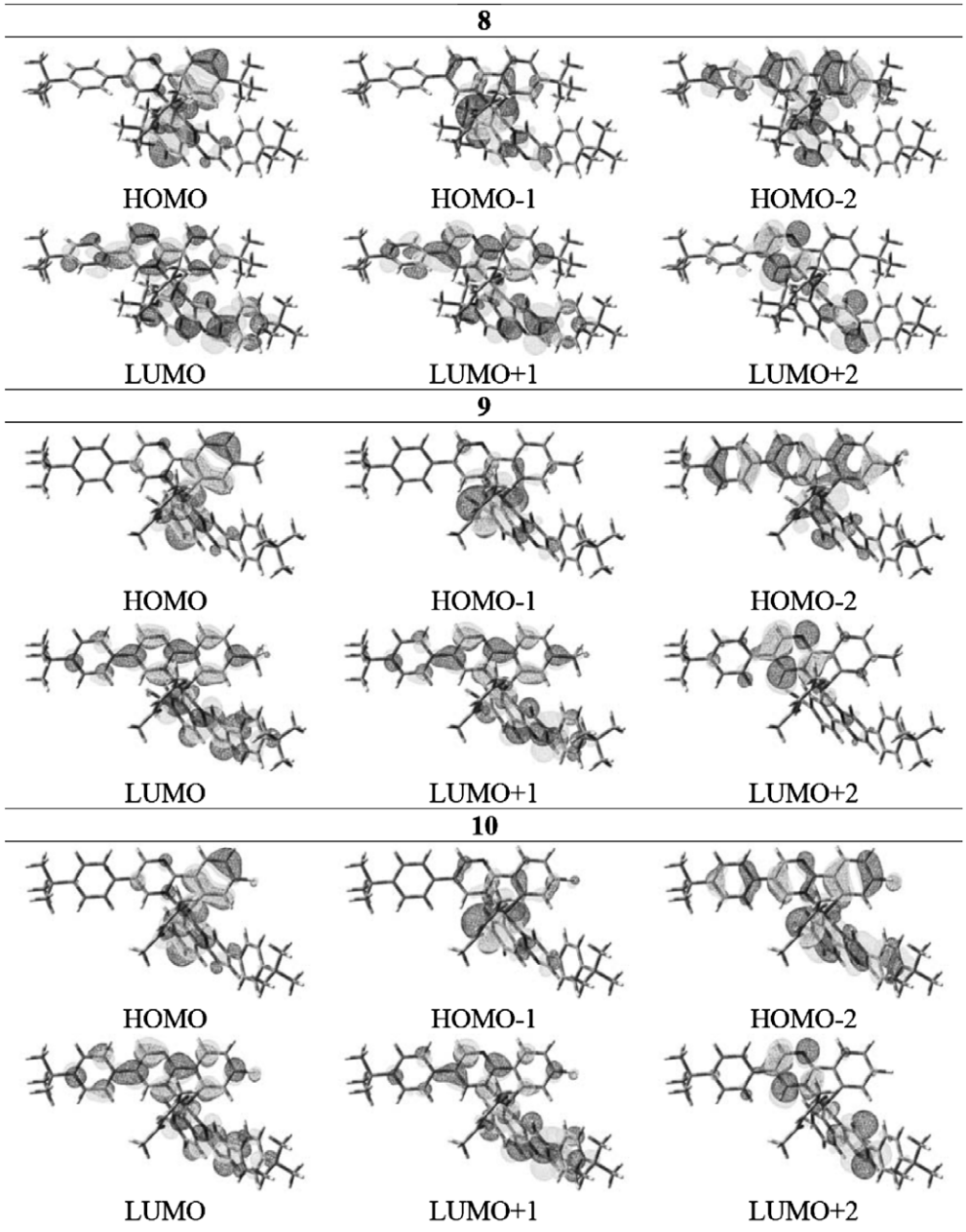

Fig. 5. Selected frontier orbitals for (**pyr**)$_2$Ir(acac).

LUMO + 1 are distributed on the whole cyclometalated ligand. The dominance of the HOMO → LUMO transition in the $S_0 \rightarrow T_1$ transition points that both MLCT and π–π* transitions have significant contributions. For complexes **8–12**, the HOMO energy level (Chart 2) is more stabilized with increasing electron-withdrawing ability of substitutents at position 3 of the cyclometalated phenyl ring: **11** (−4.82 eV) ≈ **8** (−4.84 eV) > **10** (−5.09 eV) > **9** (−5.28 eV). Furthermore, the substituent at position 4 of the cyclometalated phenyl ring has a larger effect on the HOMO energy level than that at position 3. Consequently, an electron-deficient CF_3 group at position 4 of the ligated phenyl group features more stabilizing HOMO orbital and larger energy gap of the complex than that at position 3 of the same phenyl group. This is evidenced by the lower HOMO energy (−5.36 eV) and larger energy gap (3.43 eV) of **12** compared to **9** (−5.28 and 3.35 eV). The measured oxidation potentials and bandgaps are in support of these computation results. Complexes with varied substituents at position 5' of the pyrimidine ring of **pyr**, e.g., **12–14**, have HOMO energy levels in the order of **12** (−5.36 eV) > **14** (−5.42 eV) > **13** (−5.63 eV). These results clearly meet the trend of Hammett parameters and the electrochemical data (vide supra). The order of the calculated triplet energy, **14** < **9** ≈ **8** < **13** < **11** < **10** ≈ **12**, is only slightly different from the experimental results of **14** < **8** ≈ **9** < **11** ≈ **13** < **12** < **10**.

TD-DFT calculation at the same level were also performed to give more detailed information of aforementioned complexes, and the description and energy gaps of each transition are listed in Table 2 (see computational methodology). The lowest-lying allowed transitions (S_1) are excited mainly from HOMO to LUMO/LUMO + 1 with considerable oscillator strength (0.072–0.108), assigned to the π–π* transition of **pyr** ligand. On the other hand, the two lowest-lying T_1 and T_2 transitions of all iridium analogues are constituted of transitions mainly from HOMO/HOMO − 1 to LUMO/LUMO + 1 (63–85%) and non-negligible contribution (5–7%) from HOMO − 2/HOMO − 3 to LUMO/

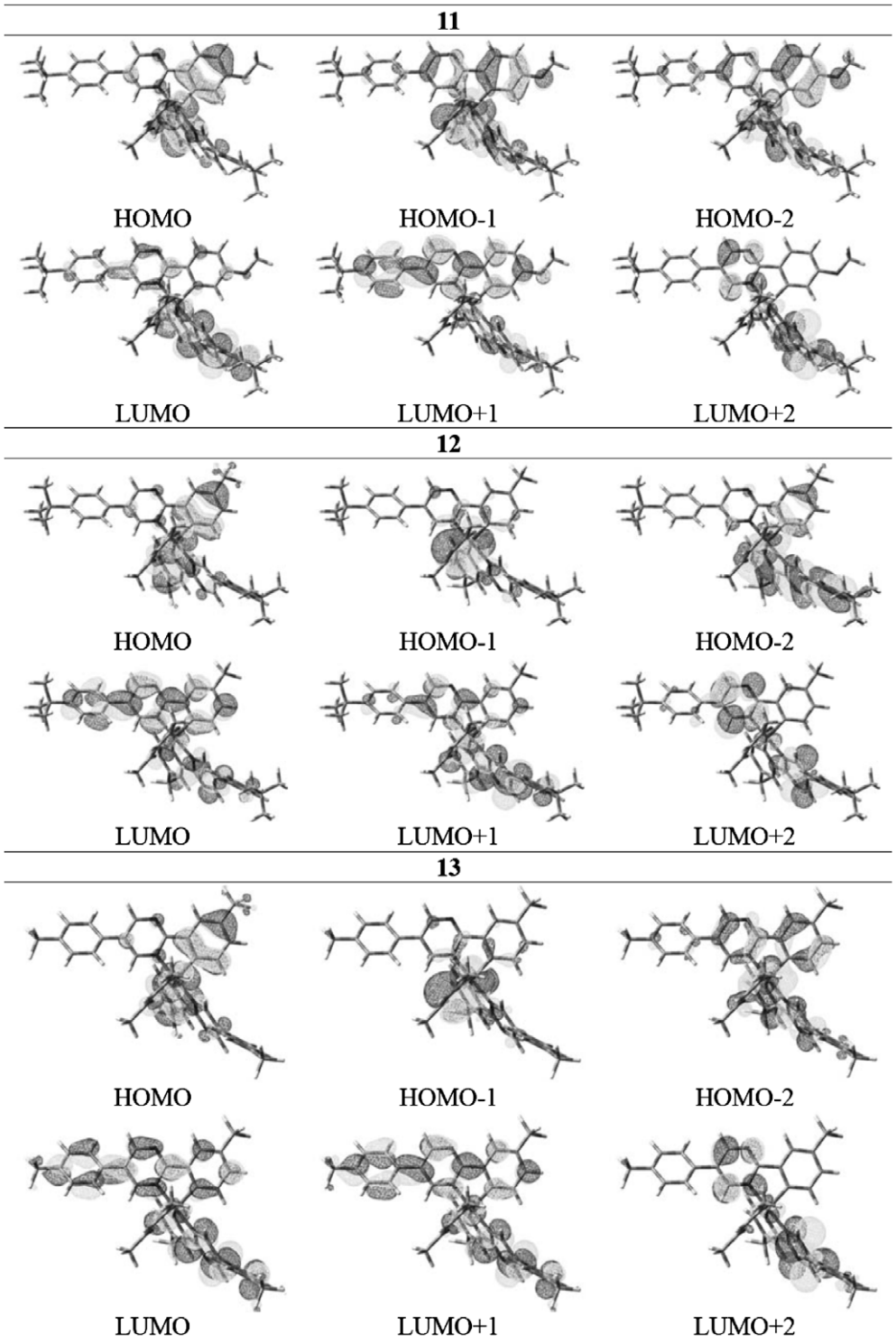

Fig. 5 *(continued)*

LUMO + 1. These are also ascribed to a mixture of ^{3}MLCT charge-transfer and ligand-centered $^3\pi\pi^*$ transitions. It is interesting that both T_1 and T_2 transitions of **11** have small contribution (17%) from HOMO − 1, indicating that the ligand-centered $^3\pi\pi^*$ transition also has some charge-transfer character because of the electron-donating nature of the methoxy group. Also, the HOMO − 1 orbital has notable contribution form the acac ligand in all complexes.

A comparison is made between the complexes in this study and their pyrimidine isomers where the non-ligated nitrogen atom of the pyrimidine is at position 5′ instead of 3′. Incorporation of a CF_3 unit at position 4′ shifts the emission to the red [16]. A homoleptic Ir complex derived from pyrimidine isomer, 3, 6-bis(phenyl)pyridazine, was reported to emit green light. The emission was tuned to red by replacement of pyridazine with phthalazine [28]. Compared to the substituent at position 3, the substituent at position 4 is expected to have more electronic influence on position 1 because HOMO has population at position 4 instead of 3. We therefore seek for the possibility of blue-shifting the λ_{em} values in these complexes by replacing the CF_3 unit in **12** with a CN unit (the complex is abbreviated as **A**). Though there is

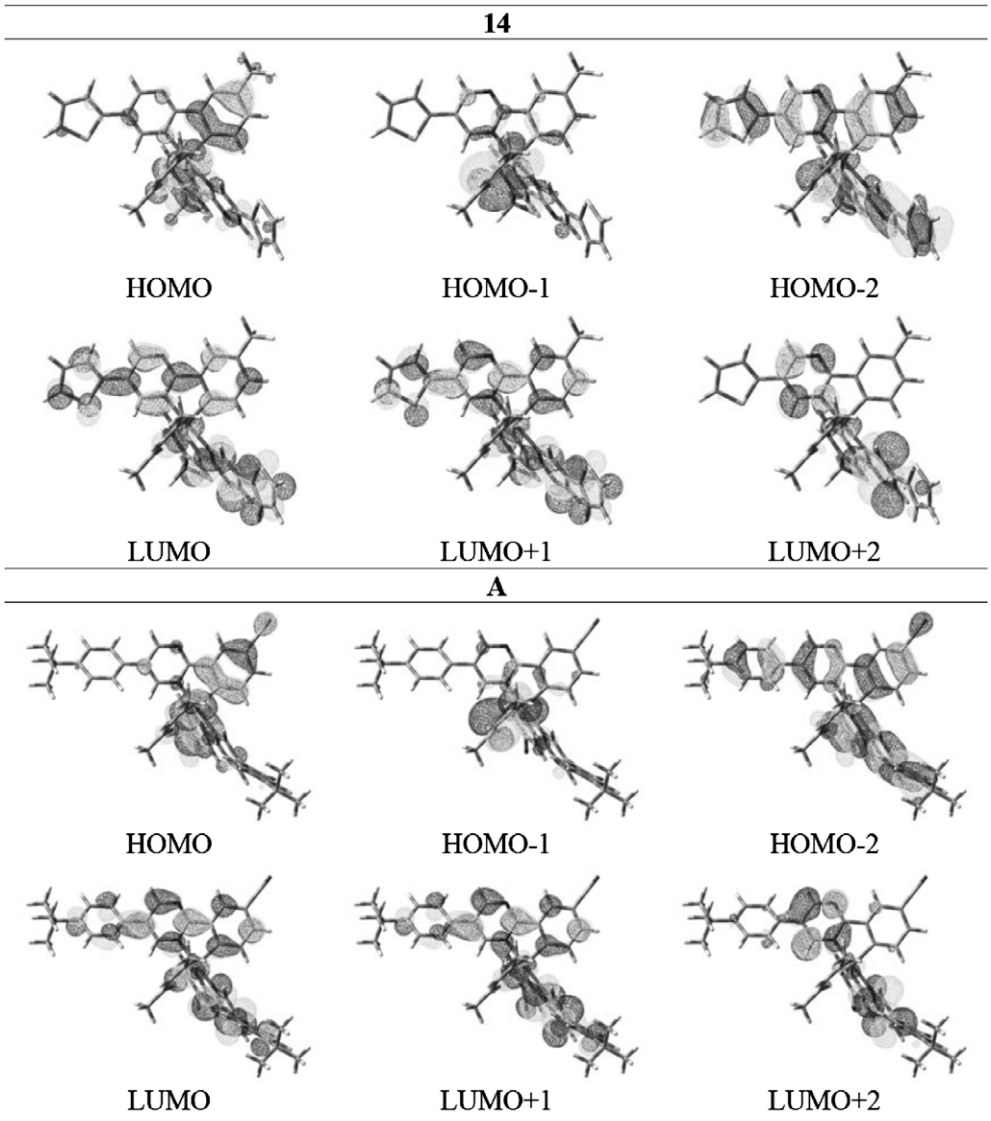

Fig. 5 *(continued)*

lowering of the HOMO level, the LUMO level is lowered by nearly the same extent (Table 2). Consequently, complexes **12** and **A** have comparable λ_{em} values. Hypsochromic shift of the emission is observed upon incorporation of an electron-donating dimethylamino unit at position 4′ of **A** (the complex is abbreviated as **B**) due to its strong inductive influence on the ligated nitrogen atom at the *para* position. More dramatic hypsochromic shift of the emission is observed only upon replacing the *tert*-butylphenyl unit at position 5' and the hydrogen atom at position 4′ of **12** by a hydrogen atom and dimethylamino unit, respectively (the complex is abbreviated as **C**). Obviously, the LUMO energy level is raised significantly upon removal of *tert*-butylphenyl unit because the LUMO is populated through the three aromatic rings in **8–14**. In contrast, a strong π-donating substituent at position 4 of the cyclometalated phenyl ring and a strong π-withdrawing substituent at position 4′ of the pyrimidine ring (Fig. 2) will have opposite effect.

2.5. Electroluminescent properties

Three of the iridium complexes were selected for device fabrication. The device structures used are similar to those in our earlier report [7a]: ITO/9,9-bis{4-[di(p-biphenyl)aminophenyl]}-fluorene (BPAPF) (40 nm)/6 wt% (**pyr**)$_2$Ir(acac) doped in 4,4′-*N*,*N*-dicarbarzolebiphenyl (CBP) (30 nm)/2,9-dimethyl-4,7-diphenyl-1,10-phenanthroline (BCP) (10 nm)/tris(8-hydroxyquinoline) aluminum (Alq_3) (30 nm)/Mg:Ag; where BPAPF [29] was used the hole-transporting layer, CBP as the host material, BCP as the hole and exciton blocking layer, and Alq_3 as the electron-transporting layer. Fig. 6 shows the configurations of the devices and the molecular structures of the compounds used in these devices.

The performance parameters of the EL devices are collected in Table 3 and the EL spectra of these devices are shown in Fig. 7. All the devices emitted light characteristic of (**pyr**)$_2$Ir(acac) which ranged from 532 to 550 nm and had narrow full width at half maximum (FWHM).

All devices exhibited turn-on voltages at 3.5−4.0 V. The device performances are shown in Figs. 8 and 9 which depicts the current–voltage–luminance properties, external quantum efficiencies, and power efficiencies versus current density, respectively. The performance of the devices at a current density of 100 mA/cm^2 is moderate: **9** (17 481 cd/m^2, 4.8%, 18 cd/A, 5.1 lm/W); **10** (18 704 cd/m^2, 4.9%, 18.9 cd/A, 4.7 lm/W); **13** (20 942 cd/m^2, 5.4%, 21.0 cd/A, 6.1 lm/W). Though the performance of the devices is better than those of normal green-emitting fluorescence OLEDs,

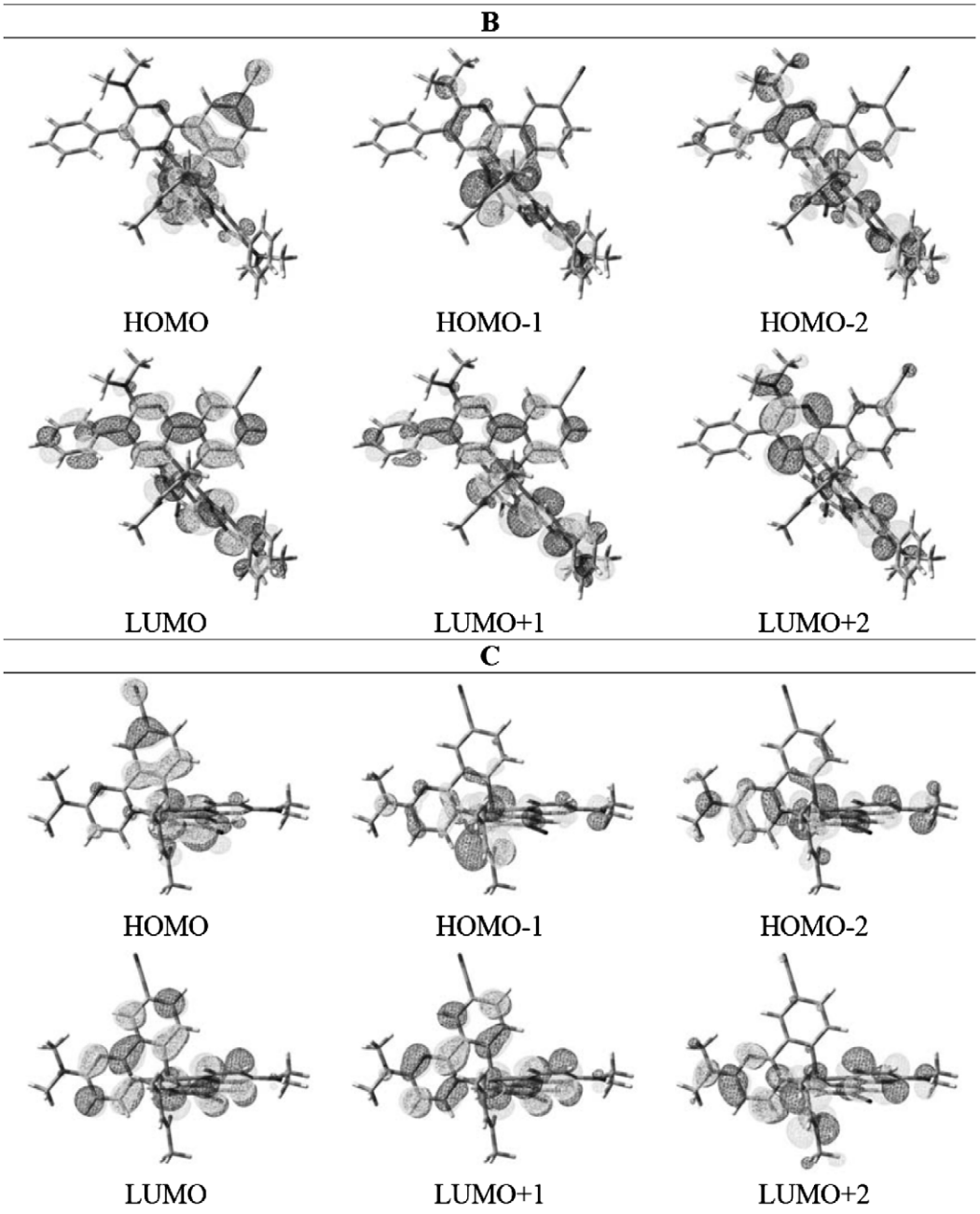

Fig. 5 *(continued)*

it is inferior to that of $(ppy)_2Ir(acac)$-based green-emitting OLED of similar device configuration [30]. With optimized device configurations, the green-emitting OLEDs based on $(ppy)_2Ir(acac)$ can have external quantum efficiency as high as ~19% [2c,31]. Such an outcome may be due to inefficient trapping of the holes in the three complexes due to their insufficiently high HOMO levels (5.50–5.92 eV) compared to that of the CBP host (HOMO = 5.5 eV), which renders direct exciton formation in the complexes less efficient. The efficiencies of the devices dropped rapidly with increased applied voltage possibly due to the increased opportunity for triplet–triplet annihilation of the phosphor-bound excitons. Therefore, optimization of the device configuration is necessary for $(\mathbf{pyr})_2Ir(acac)$ in order to have practical applications.

3. Conclusion

In summary, we have synthesized and characterized new iridium(III) complexes using pyrimidine derivatives as the cyclometalated ligands and β-diketonate as the ancillary ligand. Hammett parameters nicely rationalize the trend of the oxidation of the Ir center and the emission wavelength in these complexes. Color-tuning can be achieved via appropriate variation of the substituents at the pyridimine ligands, which is also evidenced from the computation results. The complexes emit in the range of λ_{max} = 522–558 nm in toluene with solution quantum yields ranging from 0.05 to 0.32. The EL devices using these complexes as the dopants in CBP, BPAPF and Alq_3 as the hole- and electron-transporting layers, respectively, and BCP as the hole-blocking layer, exhibited moderate perfor-

Table 2
Calculated lower-lying transitions of (**pyr**)$_2$Ir(acac).[a]

Compounds	State	Assignments[b]	E_{cal} (eV)	λ_{cal} (nm)	f[c]
8	T_1	H3 → L (6%)	2.40	517.9	0.000
		H → L (17%)			
		H → L1 (67%)			
	T_2	H → L (65%)	2.40	517.3	0.000
		H → L1 (19%)			
	S_1	H → L (79%)	2.64	470.0	0.072
		H → L1 (11%)			
		H → L2 (5%)			
	S_2	H → L (11%)	2.66	466.0	0.020
		H → L1 (80%)			
9	T_1	H3 → L1 (6%)	2.39	519.3	0.000
		H → L (83%)			
	T_2	H3 → L (7%)	2.41	514.9	0.000
		H → L1 (85%)			
	S_1	H → L (93%)	2.67	464.8	0.106
	S_2	H → L1 (92%)	2.72	456.4	0.005
10	T_1	H2 → L1 (8%)	2.48	499.9	0.000
		H → L (74%)			
	T_2	H2 → L (10%)	2.51	495.3	0.000
		H → L1 (72%)			
	S_1	H → L (89%)	2.76	449.3	0.094
		H → L2 (7%)			
	S_2	H → L1 (89%)	2.82	440.4	0.007
		H → L3 (6%)			
11	T_1	H2 → L (8%)	2.46	503.8	0.000
		H1 → L1 (17%)			
		H → L (63%)			
	T_2	H3 → L (5%)	2.47	502.3	0.000
		H2 → L1 (6%)			
		H1 → L (17%)			
		H → L1 (64%)			
	S_1	H → L (85%)	2.76	450.4	0.079
		H → L2 (10%)			
	S_2	H → L1 (88%)	2.79	444.9	0.009
		H → L3 (7%)			
12	T_1	H2 → L1 (8%)	2.49	498.9	0.000
		H → L (79%)			
	T_2	H2 → L (9%)	2.50	496.4	0.000
		H → L1 (79%)			
	S_1	H → L (91%)	2.74	452.5	0.093
		H → L2 (6%)			
	S_2	H → L1 (91%)	2.80	443.9	0.006
13	T_1	H3 → L1 (7%)	2.42	512.7	0.000
		H → L (81%)			
	T_2	H3 → L (7%)	2.43	510.0	0.000
		H → L1 (83%)			
	S_1	H → L (92%)	2.66	467.2	0.096
	S_2	H → L1 (91%)	2.71	457.5	0.007
14	T_1	H3 → L (7%)	2.34	531.4	0.000
		H2 → L1 (15%)			
		H → L (67%)			
	T_2	H3 → L1 (7%)	2.36	526.0	0.000
		H2 → L (18%)			
		H → L1 (64%)			
	S_1	H → L (93%)	2.63	471.3	0.108
	S_2	H → L1 (91%)	2.70	459.0	0.007
A	T_1	H2 → L1 (9%)	2.49	498.9	0.000
		H → L (79%)			
	T_2	H2 → L (11%)	2.51	494.8	0.000
		H → L1 (78%)			
	S_1	H → L (92%)	2.75	450.9	0.092
	S_2	H → L1 (93%)	2.81	441.2	0.007
B	T_1	H3 → L1 (5%)	2.62	473.9	0.000
		H → L (79%)			
	T_2	H3 → L (8%)	2.68	463.8	0.000
		H1 → L (6%)			
		H → L1 (69%)			
	S_1	H → L (96%)	2.88	430.6	0.107
	S_2	H → L1 (94%)	3.01	412.7	0.008
C	T_1	H → L (83%)	2.71	457.2	0.000
	T_2	H3 → L (6%)	2.77	447.7	0.000
		H → L1 (78%)			
	S_1	H → L (97%)	2.98	417.0	0.069
	S_2	H → L1 (94%)	3.09	401.1	0.001

[a] Results are based on gas-phase TD-DFT calculation.
[b] H = HOMO, L = LUMO, H1 = the next highest occupied molecular orbital, or HOMO − 1, H2 = HOMO − 2, L1 = LUMO + 1, L2 = LUMO + 2. In parentheses is the population of a pair of MO excitations.
[c] Oscillator strength.

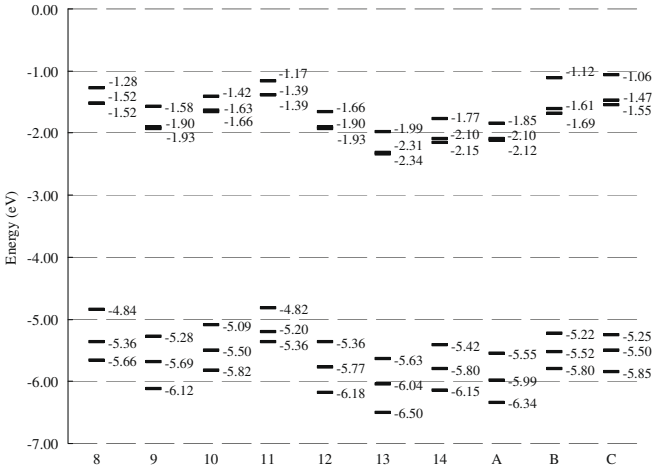

Chart 2. Schematic representation of the calculated electronic structure in the gas-phase for complexes **8–14**.

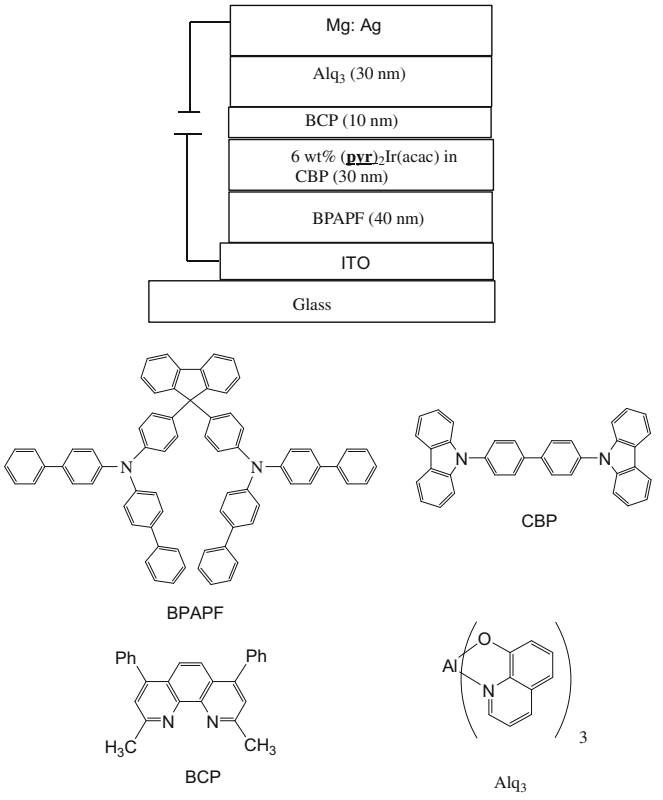

Fig. 6. The configurations of the OLED devices, and the molecular structures of the compounds used in the devices.

mance. The best performance data are found in **13**-based device: 20 942 cd/m^2, 5.4%, 21.0 cd/A, 6.1 lm/W at 100 mA/cm^2.

4. Experimental section

4.1. General information

The ^{1}H NMR spectra were recorded on a Bruker AMX400 spectrometer. FAB-mass spectra were collected on a JMS-700 double focusing mass spectrometer (JEOL, Tokyo, Japan) with a resolution of 3000 for low resolution and 8000 for high resolution (5% valley

Table 3
Electrophophorescence data for (**pyr**)$_2$Ir(acac) complexes.

Compound	**9**	**10**	**13**
V_{on} (V)	3.8	4.0	3.5
L_{max} (cd/m^2)	61 201	42 769	70 673
(V at L_{max} (V))	(15.0)	(15.0)	(15.0)
λ_{em} (nm)	550	532	542
CIE (x,y)	0.43, 0.56	0.34, 0.62	0.38, 0.60
fwhm (nm)	66	60	66
$\eta_{ext,max}$ (%)	8.46	7.44	8.02
$\eta_{p,max}$ (lm/W)	18.56	14.89	16.11
$\eta_{c,max}$ (cd/A)	30.0	28.8	31.3
L (cd/m^2)*	17 481	18 704	20 942
η_{ext} (%)*	4.8	4.9	5.4
η_p (lm/W)*	5.1	4.7	6.1
η_c (cd/A)*	18.0	18.9	21.0

L_{max}, maximum luminance; L, luminance; V_{on}, turn-on voltage; V, voltage; $\eta_{ext,max}$, maximum external quantum efficiency; $\eta_{p,max}$, maximum power efficiency; $\eta_{c,max}$, maximum current efficiency; η_{ext}, external quantum efficiency; η_p, power efficiency; η_c, current efficiency; fwhm, full width at half maximum.
* At a current density of 100 mA/cm^2.

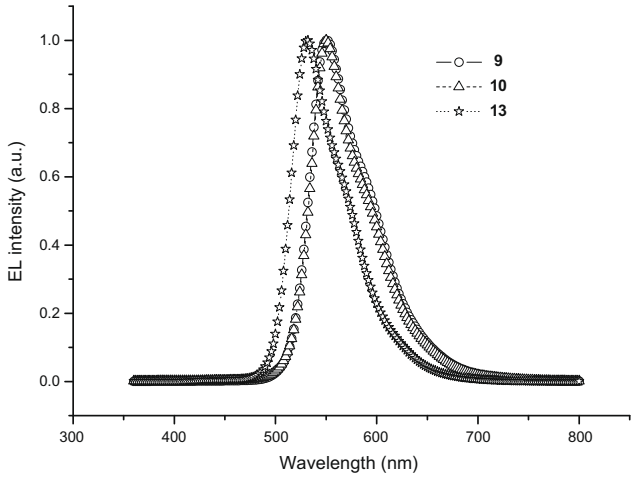

Fig. 7. EL spectra of the devices for selected complexes.

definition). For FAB-mass spectra, the source accelerating voltage was operated at 10 kV with a Xe gun, using 3-nitrobenzyl alcohol as the matrix. MALDI-mass spectra were collected on a Voyager DE-PRO (Applied Biosystem, Houston, USA) equipped with a nitrogen laser (337 nm) and operated in the delayed extraction reflector mode. Elemental analyses were performed on a Perkin–Elmer 2400 CHN analyzer. Cyclic voltammetry experiments were performed with a BHI-621B electrochemical analyzer. All measurements were carried out at room temperature with a conventional three-electrode configuration consisting of a platinum working electrode, an auxiliary electrode, and a nonaqueous Ag/AgNO$_3$ reference electrode. The $E_{1/2}$ values were determined as $1/2(E_p^a + E_p^c)$, where E_p^a and E_p^c are the anodic and cathodic peak potentials, respectively. The solvent used was CH_2Cl_2 and the supporting electrolyte was 0.1 M tetrabutylammonium hexafluorophosphate. Electronic absorption spectra were obtained on a Cary 50 Probe UV–Vis spectrometer. Emission spectra were recorded in deoxygenated solutions at 298 K by a JASCO FP-6500 fluorescence spectrometer. The emission spectra were collected on samples with o.d. $\sim$ 0.1 at the excitation wavelength. UV–Vis spectra were checked before and after irradiation to monitor any possible sample degradation. Emission maxima were reproducible within 2 nm. Luminescence quantum yields (Φ_{em}) were calculated relative to coumarin (Φ_{em} = 0.63 in acetonitrile). Luminescence quantum yields were

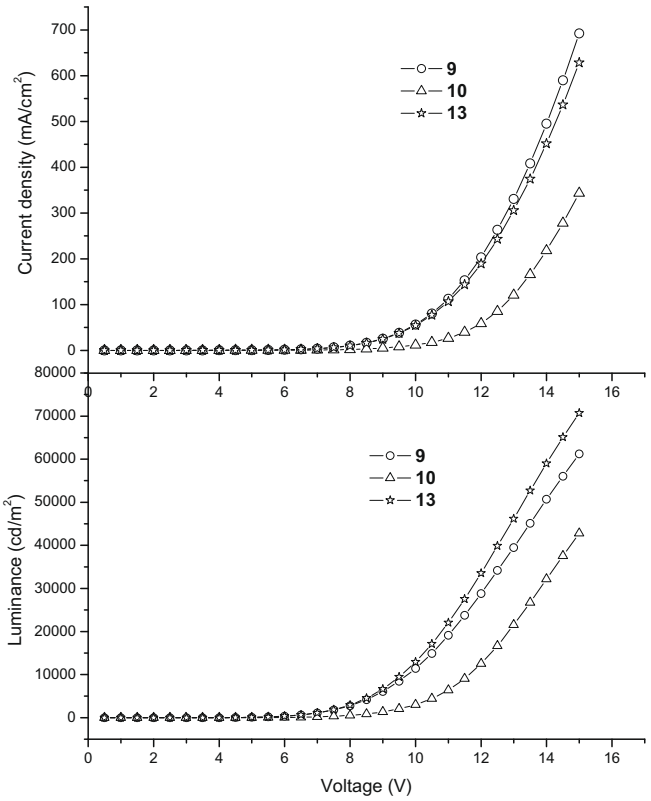

Fig. 8. I–V–L characteristics for the devices.

taken as the average of three separate determinations and were reproducible within 10%. Luminescence lifetimes were determined on an Edinburgh FL920 time-correlated pulsed single-photon-

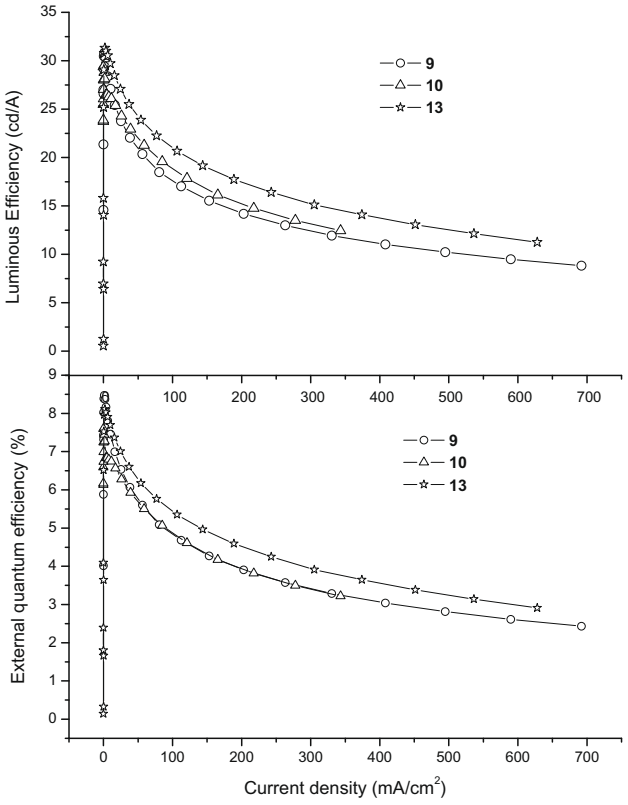

Fig. 9. External quantum efficiencies and power efficiencies of the devices.

counting instrument. Samples were degassed via freeze-thaw-pump cycle at least three times prior to measurements. Samples were excited at 337 nm from a nitrogen pulsed flashlamp with 1 ns FWHM pulse duration transmitted through a Czerny–Turner design monochromator. Emission was detected at 90° via a second Czerny–Turner design monochromator onto a thermoelectrically cooled red-sensitive photomultiplier tube. The resulting photon counts were stored on a microprocessor-based multichannel analyzer. The instrument response function was profiled using a scatter solution and subsequently deconvoluted from the emission data to yield an undisturbed decay. Nonlinear least square fittings of the decay curves were performed with the Levenburg–Marquardt algorithm and implemented by the Edinburgh Instruments F900 software. The reported values represent the average of at least three readings.

4.2. General procedure for the syntheses of pyrimidine ligands

Pyrimidine ligands were obtained via sequential palladium-catalysed Suzuki cross-coupling reactions with appropriate arylbornic acid. A mixture of arylboronic acid (10 mmol), 5-bromo-2-iodopyrimidine (2.85 g, 10 mmol), Na_2CO_3 (10 ml, 2 M in H_2O, 20 mmol), and $Pd(PPh_3)_4$ (115 mg, 1.0 mol%) and toluene (25 ml) was refluxed for 24 h under nitrogen. The resulting mixture was allowed to cool to room temperature, diluted with CH_2Cl_2 (10 mL) and extracted with brine. Combined organic extracts were dried over $MgSO_4$. The concentrated crude intermediate was purified by column chromatography on silica gel and eluted with CH_2Cl_2/hexanes. The intermediate then underwent a second Suzuki cross-coupling reaction with another arylboronic acid under similar condition except that P^tBu_3 was added as the cocatalyst.

*2,5-Bis-(4-tert-butyl-phenyl)-pyrimidine (**1**):* White powders. Yield = 70%. ^{1}H NMR (400 MHz, $CDCl_3$): δ 8.99 (s, 2H, pyrimidine), 8.38 (d, 2H, J = 8.4 Hz, C_6H_4), 7.53 (m, 6H, C_6H_4), 1.36 (s, 18H, CH_3). FABMS: *m/z* 345.2 $(M+H)^+$.

*5-(4-tert-Butyl-phenyl)-2-(4-trifluoromethyl-phenyl)-pyrimidine (**2**):* White powders. Yield = 70%. ^{1}H NMR (400 MHz, $CDCl_3$): δ 9.02 (s, 2H, pyrimidine), 8.60 (d, 2H, J = 7.6 Hz, $C_6H_4CF_3$), 7.75 (d, 2H, J = 7.6 Hz, $C_6H_4CF_3$), 7.57 (m, 4H, C_6H_4), 1.37 (s, 9H, CH_3). FABMS: *m/z* 357.2 $(M+H)^+$.

*5-(4-tert-Butyl-phenyl)-2-(4-fluoro-phenyl)-pyrimidine (**3**):* White powders. Yield = 92%. ^{1}H NMR (400 MHz, $CDCl_3$): δ 8.98 (s, 2H, pyrimidine), 8.46–8.44 (m, 2H, C_6H_4F), 7.57–7.52 (m, 4H, C_6H_4), 7.5 (td, 2H, J = 8.8 and 2.4 Hz, C_6H_4F), 1.35 (s, 9H, CH_3). FABMS: *m/z* 306.1 (M^+).

*5-(4-tert-Butyl-phenyl)-2-(4-methoxy-phenyl)-pyrimidine (**4**):* White powders. Yield = 76%. ^{1}H NMR (400 MHz, $CDCl_3$): δ 8.98 (s, 2H, pyrimidine), 8.41 (dd, 2H, J = 8.8 and 2.0 Hz, C_6H_4OMe), 7.56–7.51 (m, 4H, C_6H_4), 7.00 (dd, 2H, J = 8.8 and 2.0 Hz, $C_6H_4OCH_3$), 3.88 (s, 3H, OCH_3), 1.36 (s, 9H, CH_3). FABMS: *m/z* 319.2 $(M+H)^+$.

*5-(4-tert-Butyl-phenyl)-2-(3-trifluoromethyl-phenyl)-pyrimidine (**5**):* White powders. Yield = 73%. ^{1}H NMR (400 MHz, $CDCl_3$): δ 9.02 (s, 2H, pyrimidine), 8.82 (s, 1H, $C_6H_4CF_3$), 8.66 (d, 1H, J = 7.6 Hz, $C_6H_4CF_3$), 7.73 (d, 1H, J = 7.6 Hz, $C_6H_4CF_3$), 7.58 (m, 5H, C_6H_4 and $C_6H_4CF_3$), 1.37 (s, 9H, CH_3). FABMS: *m/z* 357.1 $(M+H)^+$.

*2-(3-Trifluoromethyl-phenyl)-5-(4-trifluoromethyl-phenyl)-pyrimidine (**6**):* White powders. Yield = 67%. ^{1}H NMR (400 MHz, $CDCl_3$): δ 9.04 (s, 2H, pyrimidine), 8.79 (s, 1H, $C_6H_4CF_3$), 8.69 (d, 1H, J = 7.6 Hz, $C_6H_4CF_3$), 7.76 (m, 5H, $C_6H_4CF_3$ and C_6H_4), 7.63 (t, 1H, J = 8.0 Hz, $C_6H_4CF_3$). FABMS: *m/z* 369.1 $(M+H)^+$.

*5-Thiophen-2-yl-2-(3-trifluoromethyl-phenyl)-pyrimidine (**7**)*: White powders. Yield = 65%.^{1}H NMR (400 MHz, $CDCl_3$): δ 9.02 (s, 2 H, pyrimidine), 8.75 (s, 1H, $C_6H_4CF_3$), 8.65 (d, 1H, J = 7.6 Hz, $C_6H_4CF_3$), 7.73 (d, 1H, J = 7.6 Hz, $C_6H_4CF_3$), 7.61 (t, 1H, J = 7.6 Hz, $C_6H_4CF_3$), 7.45–7.44 (m, 2H, thiophene), 7.17 (t, 1H, J = 4.0 Hz, thiophene). FABMS: *m/z* 307.2 $(M+H)^+$.

4.3. General procedure for the synthesis of (**pyr**)$_2$Ir(acac)

To a flask containing $IrCl_3{\cdot}nH_2O$ (176 mg, 0.50 mmol) and 1.0 equiv. of **pyr** ligands, a 3:1 mixture of 2-ethoxyethanol and water (25 mL) was added. The mixture was then refluxed for 48 h and cooled to room temperature. After cooling, the reaction was quenched by water and the resulting mixture was washed with acetone and hexanes. The solid formed was collected by filtration and pumped dry to give the crude product of the μ-chloro-bridged Ir(III) dimer. This crude product was mixed with Na_2CO_3 (0.30 g, 3.0 mmol), 2,4-pentanedione (0.30 g, 3.0 mmol) and 2-methoxyethanol (20 mL) in a flask. The mixture was then heated to reflux for 24 h. After cooling, the reaction was quenched by water and the mixture was extracted with CH_2Cl_2. The combined extracts were then washed with brine, dried over $MgSO_4$, and evaporated to dryness. The crude product was purified by column chromatography on a silica gel column using a mixture of CH_2Cl_2 and hexanes (1:1 by volume) as the eluent.

*Compound **8**:* Orange powders. Yield = 12%. ^{1}H NMR (400 MHz, $CDCl_3$): δ 8.95 (d, 2H, J = 2.8 Hz, pyrimidine), 8.89 (d, 2H, J = 2.8 Hz, pyrimidine), 7.84 (d, 2H, J = 8.4 Hz, C_6H_3), 7.56 (s, 8H, C_6H_4), 6.93 (d, 2H, J = 8.4 Hz, C_6H_3), 6.33 (s, 2H, C_6H_3), 5.19 (s, 1H, acac-CH), 1.79 (s, 6H, acac-CH_3), 1.37 (s, 18H, CH_3), 1.05 (s, 18H, CH_3). FABMS: *m/z* 978.4 (M^+). Anal. Calc. for $C_{53}H_{61}N_4O_2Ir$: C, 65.07; H, 6.28; N, 5.73. Found: C, 64.86; H, 6.08; N, 5.71%.

*Compound **9**:* Yellow–orange powders. Yield = 21%. ^{1}H NMR (400 MHz, $CDCl_3$): δ 9.06 (s, 2H, pyrimidine), 8.86 (s, 2H, pyrimidine), 8.07 (d, 2H, J = 8.4 Hz, $C_6H_3CF_3$), 7.58 (d, 8H, J = 1.2 Hz, $C_6H_4CF_3$), 7.14 (d, 2H, J = 8.4 Hz, $C_6H_3CF_3$), 6.52 (s, 2H, $C_6H_3CF_3$), 5.28 (s, 1H, acac-CH), 1.82 (s, 6H, acac-CH_3), 1.37 (s, 18H, CH_3). FABMS: *m/z* 1002.0 (M^+). Anal. Calc. for $C_{47}H_{43}F_6N_4O_2Ir$: C, 56.33; H, 4.33; N, 5.59. Found: C, 56.07; H, 4.21; N, 5.38%.

*Compound **10**:* Yellow powders. Yield = 12%. ^{1}H NMR (400 MHz, $CDCl_3$): δ 8.99 (d, 2H, J = 2.8 Hz, pyrimidine), 8.79 (d, 2H, J = 2.8 Hz, pyrimidine), 7.98 (td, 2H, J = 8.8 and 2.4 Hz, C_6H_3F), 7.57 (s, 8H, C_6H_4), 6.62 (td, 2H, J = 8.8 and 2.4 Hz, C_6H_3F), 5.98 (d, 1H, J = 2.4 Hz, C_6H_3F), 5.96 (d, 1H, J = 2.4 Hz, C_6H_3F), 5.30 (s, 1H, acac-CH), 1.82 (s, 6H, acac-CH_3), 1.37 (s, 18H, CH_3). FABMS: *m/z* 902.2 (M^+). Anal. Calc. for: $C_{45}H_{43}F_2N_4O_2Ir$: C, 59.92; H, 4.80; N, 6.21. Found: C, 60.09; H, 4.60; N, 6.00%.

*Compound **11**:* Yellow powders. Yield = 31%. H NMR (400 MHz, $CDCl_3$): δ 8.92 (d, 2H, J = 2.8 Hz, pyrimidine), 8.80 (d, 2H, J = 2.8 Hz, pyrimidine), 7.91 (d, 2H, J = 8.4 Hz, C_6H_3), 7.55 (s, 8H, C_6H_4), 6.49 (d, 2H, J = 8.4 Hz, C_6H_3), 5.87 (s, 2H, C_6H_3), 5.22 (s, 1H, acac-CH), 3.57 (s, 6H, OCH_3), 1.81 (s, 6H, acac-CH_3), 1.37 (s, 18H, CH_3). FABMS: *m/z* 926.2 (M^+). Anal. Calc. for: $C_{47}H_{49}N_4O_4Ir$: C, 60.95; H, 5.33; N, 6.05. Found: C, 60.70; H, 4.97; N, 5.75%.

*Compound **12**:* Yellow powders. Yield = 12%. ^{1}H NMR (400 MHz, $CDCL_3$): δ 9.06 (d, 2H, J = 2.8 Hz, pyrimidine), 8.86 (s, 2H, J = 2.8 Hz, pyrimidine), 8.23 (s, 2H, $C_6H_3CF_3$), 7.58 (s, 8H, C_6H_4), 6.99 (d, 2H, J = 8.0 Hz, $C_6H_3CF_3$), 6.47 (d, 2H, J = 8.0 Hz, $C_6H_3CF_3$), 5.28 (s, 1 H, acac-CH), 1.82 (s, 6H, acac-CH_3), 1.37 (s, 18H, CH_3). FABMS: *m/z* 1002.5 (M^+). Anal. Calc. for: $C_{47}H_{43}F_2F_6N_4O_2Ir$: C, 56.33; H, 4.33; N, 5.59. Found: C, 56.73; H, 4.49; N, 5.43%.

*Compound **13**:* Yellow powders. Yield = 26%. ^{1}H NMR (400 MHz, $CDCl_3$): δ 9.09 (d, 2H, J = 2.8 Hz, pyrimidine), 8.86 (d, 2H, J = 2.8 Hz, pyrimidine), 8.27 (s, 2H, $C_6H_3CF_3$), 7.86–7.73 (m, 8H, $C_6H_4CF_3$), 7.03 (d, 2H, J = 8.0 Hz, $C_6H_3CF_3$), 6.47 (d, 2H, J = 8.0 Hz, $C_6H_3CF_3$), 5.32 (s, 1 H, acac-CH), 1.84 (s, 6H, acac-CH_3). FABMS: *m/z* 1026.2 (M^+). Anal. Calc. for $C_{41}H_{25}F_{12}N_4O_2Ir$: C, 48.00; H, 2.46; N, 5.46. Found: C, 48.12; H, 2.41; N, 5.42%.

*Compound **14**:* Orange powders. Yield = 22%. ^{1}H NMR (400 MHz, $CDCl_3$): δ 9.05 (d, 2H, J = 2.8 Hz, pyrimidine), 8.83 (d, 2H, J = 2.8 Hz, pyrimidine), 8.21 (s, 2H, $C_6H_3CF_3$), 7.47 (m, 4H, thiophene), 7.19 (t, 2H, J = 3.6 Hz, thiophene), 7.00 (d, 2H, J = 8.0 Hz, $C_6H_3CF_3$), 6.47 (d, 2H, J = 8.0 Hz, $C_6H_3CF_3$), 5.31 (s, 1H, acac-CH), 1.87 (s, 6H, acac-

CH_3). FABMS: *m/z* 901.9 (M^+). Anal. Calc. for $C_{35}H_{23}F_6N_4O_2S_2Ir$: C, 46.61; H, 2.57; N, 6.21. Found: C, 46.73; H, 2.74; N, 5.96%.

4.4. LEDs fabrication and measurements

Compound BCP (2.9-dimethyl-4,7-diphenyl-1,10-phenanthroline) was purchased from Aldrich and used as received. Compounds Alq_3 (tris(8-hydroxyquinoline)aluminum) [32], CBP (4,4′-*N*,*N*″-dicarbazolebiphenyl) [33], and BPAPF (9,9-bis{4-{di(*p*-biphenyl)aminophenyl}}fluorene) [29] were synthesized according to literature procedures, and were sublimed twice prior to use. Prepatterned ITO substrates with an effective individual device area of 3.14 mm^2 were cleaned as described in a previous report [34]. A 40-nm-thick film of BPAPF was deposited first as the hole transport layer (HTL). The light-emitting layer (30 nm) was then deposited by coevaporating the CBP host and the phosphorescent dopant (~6% dopant concentration), with both deposition rates being monitored by two independent quartz crystal oscillators. A 10-nm-thick BCP as the hole and exciton blocking layer (HBL) and 30-nm-thick Alq_3 as the electron transport layer were then deposited sequentially. Finally, an alloy of magnesium and silver (ca. 10:1, 500 Å) was deposited as the cathode, which was capped with 1000 Å of silver. *I–V* curve was measured on a Keithley 2400 Source meter in ambient environment. Light intensity was measured with a Newport 1835 optical meter.

4.5. Computational methodology

Geometrical optimization of the molecules at density functional level was carried out with Q-Chem [27] software using B3LYP exchange-correlation functional. The CRENBL basis set with relativistic effective potential is applied to the iridium atom [35], where 6-31G* basis set is applied to the rest of the atoms. The gas-phase time-dependent DFT (TD-DFT) calculations at the same level were performed on the basis of the geometry in the ground state. TD-DFT calculations were previously employed to characterize excited states with charge-transfer character [36]. In some cases underestimation of the excitation energies was observed [36,37]. We have also performed the TD-DFT calculations at the same level using GAUSSIAN 03 program suite. The results show that inclusion of the solvent effect, e.g., toluene, CH_2Cl_2 and acetonitrile, only slightly affect the λ_{cal} despite using either PCM or C-PCM solvation model. Therefore, in the present work, we use TD-DFT (calculated with Q-Chem) to characterize the electronic configuration and avoid drawing conclusions from the excitation energy.

Acknowledgements

We gratefully acknowledge support from the National Science Council, Academia Sinica, and National Central University.

References

[1] (a) E. Holder, B.M.W. Langeveld, U.S. Schubert, Adv. Mater. 17 (2005) 1109;
(b) R.C. Evans, P. Douglas, C.J. Winscom, Coord. Chem. Rev. 250 (2006) 2093;
(c) P.-T. Chou, Y. Chi, Chem. Eur. J. 13 (2007) 380.
[2] (a) M.A. Baldo, D.F. O'Brien, Y. You, A. Shoustikov, S. Sibley, M.E. Thompson, S.R. Forrest, Nature 395 (1998) 151;
(b) M.A. Baldo, D.F. O'Brien, M.E. Thompson, S.R. Forrest, Phys. Rev. B 60 (1999) 14422;
(c) C. Adachi, M.A. Baldo, M.E. Thompson, S.R. Forrest, J. Appl. Phys. 90 (2001) 5048.
[3] (a) T. Tsuzuki, N. Shirasawa, T. Suzuki, S. Tokito, Adv. Mater. 15 (2003) 1455;
(b) J. Li, P.I. Djurovich, B.D. Alleyne, M. Yousufuddin, N.N. Ho, J.C. Thomas, J.C. Peters, R. Bau, M.E. Thompson, Inorg. Chem. 44 (2005) 1713;
(c) C.-J. Chang, C.-H. Yang, K. Chen, Y. Chi, C.-F. Shu, M.-L. Ho, Y.-S. Yeh, P.-T. Chou, J. Chem. Soc., Dalton Trans. (2007) 1881;
(d) C.-F. Chang, Y.-M. Cheng, Y. Chi, Y.-C. Chiu, C.-C. Lin, G.-H. Lee, P.-T. Chou, C.-C. Chen, C.-H. Chang, C.-C. Wu, Angew. Chem. Int. Ed. 47 (2008) 4542.
[4] (a) C. Adachi, R.C. Kwong, P. Djurovich, V. Adamovich, M.A. Baldo, M.E. Thompson, S.R. Forrest, Appl. Phy. Lett. 79 (2001) 2082;
(b) R. Ragni, E.A. Plummer, K. Brunner, J.W. Hofstraat, F. Babudri, G.M. Farinola, F. Naso, L.D. Cola, J. Mater. Chem. 16 (2006) 1161;
(c) R.N. Bera, N. Cumpstey, P.L. Burn, I.D.W. Samuel, Adv. Funct. Mater. 17 (2007) 1149;
(d) S.C. Lo, N.A.H. Male, J.P.J. Markham, S.W. magennis, P.L. Burn, O.V. Salata, I.D.W. Samuel, Adv. Mater. 14 (2002) 975.
[5] J.P. Puan, P.P. Sun, C.H. Cheng, Adv. Mater. 15 (2003) 224.
[6] S.C. Lo, C.P. Shipley, R.N. Bera, R.E. Harding, A.R. Cowley, P.L. Burn, I.D.F. Samuel, Chem. Mater. 18 (2006) 5119.
[7] (a) W.-S. Huang, J.T. Lin, C.-H. Chien, Y.-T. Tao, S.-S. Sun, Y.-S. Wen, Chem. Mater. 16 (2004) 2480;
(b) W.-S. Huang, J.T. Lin, H.-C. Lin, Org. Electron. 9 (2008) 557;
(c) J. Ding, J. Gao, Y. Cheng, Z. Xie, L. Wang, D. Ma, X. Jing, F. Wang, Adv. Funct. Mater. 16 (2006) 575.
[8] D. Kolosov, V. Adamovich, P. Djurovich, M.E. Thompson, C. Adachi, J. Am. Chem. Soc. 124 (2002) 9945.
[9] (a) C.Y. Jiang, W. Yang, J.B. Peng, S. Xiao, Y. Cao, Adv. Mater. 16 (2004) 537;
(b) Y. Kawamura, S. Yanagida, S.R. Forrest, J. Appl. Phys. 92 (2002) 87.
[10] M. Velusamy, K.R. Justin Thomas, C.-H. Chen, J.T. Lin, Y.S. Wen, W.-T. Hsieh, C.-H. Lai, P.-T. Chou, J. Chem. Soc., Dalton Trans. (2007) 3025.
[11] K.R. Justin Thomas, M. Velusamy, J.T. Lin, C.-H. Chien, Y.-T. Tao, Y.S. Wen, Y.-H. Hu, P.-T. Chou, Inorg. Chem. 44 (2005) 5677.
[12] T. Kulikowski, Pharmacy World and Science 16 (1994) 127.
[13] (a) H. Zaschke, J. Prakt. Chem. 317 (1975) 617;
(b) T. Geelhaar, Ferroelectrics 85 (1988) 329;
(c) S.M. Kelly, J. Funfschilling, J. Mater. Chem. 3 (1993) 953;
(d) M. Hird, K.J. Toyne, G.W. Gray, Liq. Cryst. 14 (1993) 741;
(e) A. Sakaigawa, H. Nohira, Ferroelectrics 148 (1993) 71;
(f) M. Bremer, Adv. Mater. 7 (1995) 803.
[14] (a) K.-T. Wong, T.S. Hung, Y. Lin, C.-C. Wu, G.-H. Lee, S.-M. Peng, C.H. Chou, Y.O. Su, Org. Lett. 4 (2002) 513;
(b) C. Wang, G.-Y. Jung, A.S. Batsanov, M.R. Bryce, M.C. Petty, J. Mater. Chem. 12 (2002) 173.
[15] (a) S.-J. Su, D. Tanaka, Y.-J. Li, H. Sasabe, T. Takeda, J. Kido, Org. Lett. 10 (2008) 941;
(b) S.-J. Su, T. Chiba, T. Takeda, J. Kido, Adv. Mater. 20 (2008) 2125.
[16] (a) Y.-H. Niu, B. Chen, S. Liu, H. Yip, J. Bardecker, A.K.-Y. Jen, J. Kavitha, Y. Chi, C.-F. Shu, Y.-H. Tseng, C.-H. Chien, Appl. Phys. Lett. 85 (2004) 1619;
(b) C.-H. Yang, C.-H. Chen, I.-W. Sun, Polyhedron 25 (2006) 2407.
[17] J.H. Goodby, M. Hied, R.A. Lewis, K.J. Toyne, Chem. Commun. (1996) 2719.
[18] J. Pommerehne, H. Vestweber, W. Guss, R.F. Mahrt, H. Bässler, M. Porsch, J. Daub, Adv. Mater. 7 (1995) 551.
[19] J. Brooks, Y. Babayan, S. Lamansky, P.I. Djurovich, I. Tsyba, R. Bau, M.E. Thompson, Inorg. Chem. 41 (2002) 3055.
[20] S. Lamansky, P. Djurovich, D. Murphy, F. Abdel-Razzaq, R. Kwong, I. Tsyba, M. Bortz, M.B. Mui, B.R. Bau, M.E. Thompson, Inorg. Chem. 40 (2001) 1704.
[21] V.V. Grushin, N. Herron, D.D. LeCloux, W.J. Marshall, V.A. Petrov, Y. Wang, Chem. Commun. (2001) 1494.
[22] A.B. Tamayo, B.D. Alleyne, P.I. Djurovich, S. Lamansky, I. Tsyba, N.N. Ho, R. Bau, M.E. Thompson, J. Am. Chem. Soc. 125 (2003) 7377.
[23] (a) Y. Ohsawa, S. Sprouse, K.A. King, M.K. DeArmond, K.W. Hanck, R.J. Watts, J. Phys. Chem. 91 (1987) 1047;
(b) F.O. Garces, K.A. King, R.J. Watts, Inorg. Chem. 27 (1988) 3464.
[24] P.J. Hay, J. Phys. Chem. A 106 (2002) 634.
[25] E.V. Anslyn, D.A. Dougherty, Modern Physical Organic Chemistry, University Science Books, California, 2006.
[26] P. Coppo, E.A. Plummer, L.D. Cola, Chem. Commun. (2004) 1774.
[27] (a) N. Hirata, J.-J. Lagref, E.J. Palomares, J.R. Durrant, M.K. Nazeeruddin, M. Grätzel, D. Di Censo, Chem. Eur. J. 10 (2004) 595;
(b) J.R. Durrant, S.A. Haque, E. Palomares, Chem. Commun. (2006) 3279;
(c) Y. Shao, L.F. Molnar, Y. Jung, J. Kussmann, C. Ochsenfeld, S.T. Brown, A.T.B. Gilbert, L.V. Slipchenko, S.V. Levchenko, D.P. O'Neill, R.A. DiStasio Jr., R.C. Lochan, T. Wang, G.J.O. Beran, N.A. Besley, J.M. Herbert, C.Y. Lin, T.V. Voorhis, S.H. Chien, A. Sodt, R.P. Steele, V.A. Rassolov, P.E. Maslen, P.P. Korambath, R.D. Adamson, B. Austin, J. Baker, E.F.C. Byrd, H. Dachsel, R.J. Doerksen, A. Dreuw, B.D. Dunietz, A.D. Dutoi, T.R. Furlani, S.R. Gwaltney, A. Heyden, S. Hirata, C.-P. Hsu, G. Kedziora, R.Z. Khalliulin, P. Klunzinger, A.M. Lee, M.S. Lee, W.Z. Liang, I. Lotan, N. Nair, B. Peters, E.I. Proynov, P.A. Pieniazek, Y.M. Rhee, J. Ritchie, E. Rosta, C.D. Sherrill, A.C. Simmonett, J.E. Subotnik, H.L. Woodcock III, W. Zhang, A.T. Bell, A.K. Chakraborty, Phys. Chem. Chem. Phys. 8 (2006) 3172.
[28] B.X. Mi, P.F. Wang, Z.Q. Gao, C.S. Lee, S.T. Lee, H.L. Hong, X.M. Chen, M.S. Wong, P.F. Xia, K.W. Cheah, C.H. Chen, W. Huang, Adv. Mater. 21 (2009) 339.
[29] C.-W. Ko, Y.-T. Tao, Synth. Met. 126 (2002) 37.
[30] S. Lamansky, P. Djurovich, D. Murphy, F. Abdel-Razzaq, H.-E. Lee, C. Adachi, P.E. Burrows, S.R. Forrest, M.E. Thompson, J. Am. Chem. Soc. 123 (2001) 4304.
[31] M. Ikai, S. Tokito, Y. Sakamoto, T. Suzuki, Y. Taga, Appl. Phys. Lett. 79 (2001) 156.
[32] C.H. Chen, J. Shi, Coord. Chem. Rev. 171 (1998) 161.

[33] B.E. Koene, D.E. Loy, M.E. Thompson, Chem. Mater. 10 (1998) 2235.
[34] E. Balasubramaniam, Y.T. Tao, A. Danel, P. Tomasik, Chem. Mater. 12 (2000) 2788.
[35] L.A. LaJohn, P.A. Christiansen, R.B. Ross, T. Atashroo, W.C. Ermler, J. Chem. Phys. 87 (1987) 2812.
[36] (a) H.M. Vaswani, C.-P. Hsu, M. Head-Gordon, G.R. Fleming, J. Phys. Chem. B 107 (2003) 7940;
(b) Y. Kurashige, T. Nakajima, S. Kurashige, K. Hirao, Y. Nishikitani, J. Phys. Chem. A 111 (2007) 5544.
[37] A. Dreuw, M. Head-Gordon, J. Am. Chem. Soc. 126 (2004) 4007.